4.
FLOWER-SHAPED PLANAR MONOPOLE ANTENNA

4.1 Introduction

Though there are many advantages of non-planar broadband antennas but they are inefficient for handheld mobile communication devices. The trapezoidal toothed log-periodic antenna (TTLPA) investigated in previous chapter is bigger in size and suffers from complexity of integration with other planar circuit components. Therefore, the planar antennas designed using printed circuit board (PCB) technology are most suitable for handheld mobile communication devices. With the development of modern wireless communication systems, the need for the design and development of compact broadband planar antennas, which can fit in the portable broadband systems, has increased tremendously in recent years. Owing to their inherent properties including planar structure, compact size, easy mountability on planar surfaces, simple low-cost manufacturing, and near omni-directional radiation pattern, microstrip patch antennas are promising candidates as planar and compact transmitting/receiving elements for portable systems [Garg *et al.* (2001) and Kumar and Ray (2003)]. However, conventional microstrip patch antennas cannot be used for such purposes due to their narrow bandwidth characteristic, which was also discussed in chapter 1. To mitigate this problem, various techniques are reported in the literatures which make the microstrip patch antenna wider in impedance bandwidth. The detailed review concerning the techniques employed for bandwidth enhancement of planar monopole antennas (PMAs) is given in chapter 2. Some of the recently reported bandwidth enhancement techniques include the use of parasitic elements [Abdelaziz (2006)], slot loading [Chen *et al.* (2009)], shorting posts [Abbaspur and Hassani (2008)], fractal geometry [Shambavi and Alex (2014)], electromagnetic band gap structures [Gujral *et al.* (2012)], and metamaterials [Xiong *et al.* (2012)], which result in complex antenna geometry. On the other hand, simple techniques are also reported for this purpose in which slight modification of patch and the use of partial ground plane are involved [Deng *et al.* (2009)].

Out of these patch antennas of different shapes, some patch geometries are inspired by naturally occurring leaves and flowers [Lotfi Neyestanak (2008), Tang *et al.* (2014), and Naser-Moghadasi *et al.* (2015)]. Due to their smooth curvature and distinct sub-sections, the patch geometries inspired by nature are very promising for making this type of antenna broadband and compact. The antennas having natural shapes can provide broad bandwidth when excited using proper feeds and supporting matching circuits. The shape of conventional circular patch can be modified to a natural shape so that it contains distinct smaller segments and larger perimeter without changing the size of patch. The distinct smaller segments provide higher resonant frequencies while the larger perimeter shifts the first resonant frequency and lower cutoff frequency towards lower frequency side. This concept can be utilized in designing a compact and broadband patch antenna by using proper feed for excitation. Microstrip line (MS) and coplanar waveguide (CPW) feeds are used for such purposes, because their ground planes when modified can act as impedance matching networks. The shape and dimensions of the ground plane can be optimized so that the modified patch antenna can provide broad bandwidth.

The planar monopole antennas (PMAs) are much sought after antennas for the modern wireless communication systems since the release of an unlicensed frequency spectrum of 7.5 GHz bandwidth over the frequency range 3.1−10.6 GHz, designated as ultra wideband spectrum [FCC (2002)]. The PMAs suitable for UWB application (also known as UWB antennas) have become the subject of recent research in both academic and industry sectors. The UWB system refers to any radio system that has a -10 dB reflection coefficient bandwidth larger than 25 % of its center frequency, or has a -10 dB reflection coefficient bandwidth equal to or larger than 1.5 GHz, if the center frequency is greater than 6 GHz [Kim and Park (2006)]. The UWB systems have the potential to provide high data-rates, high resolution and good target characterization in such applications as indoor short range communications, imaging, and surveillance [Liu *et al.* (2014)].

In this chapter, flower-shaped PMA, which is a modified form of conventional circular patch is proposed to provide broad bandwidth. The proposed flower-shaped PMA is studied using two types of feed: CPW and tapered microstrip line along with semielliptical partial ground plane. The design and simulation of the proposed antenna were carried out using Ansys' HFSS software. The proposed antenna along with feed line of optimized dimensions (obtained through simulation) were fabricated and tested. The experimental results for input and radiation characteristics as well as group delay-frequency characteristic of the proposed antenna using each type of feed are compared with the respective simulation results. Further, the performance comparison of the proposed antenna fed through CPW and microstrip line is also done.

4.2 Design of Flower-shaped Patch

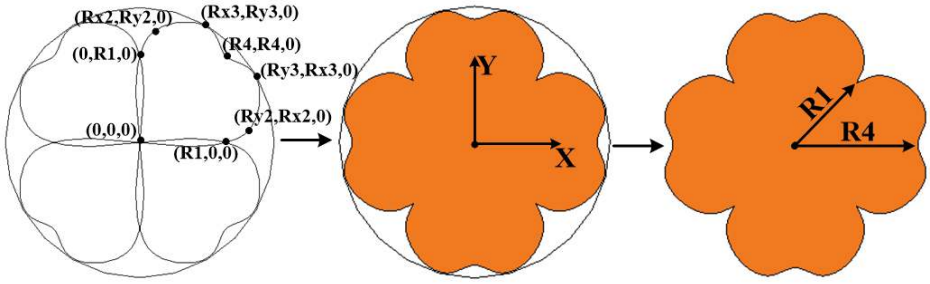

Figure 4.1: Design methodology of flower-shape (a) spline based curves, (b) comparison of circular and flower-shaped patches, and (c) flower-shaped patch along with its important geometrical parameters.

It is well known that first resonant frequency is inversely proportional to perimeter of patch [Fakharian and Rezaei (2014)]. If first resonant frequency of the antenna is to be reduced, the perimeter of the antenna has to be increased without affecting the overall size of the antenna. Different shapes available in nature, such as the shape of trees, leaves and flowers can be taken for innovative design of microstrip patch. In the proposed microstrip antenna, the conventional circular patch is modified to flower-shaped patch, which has larger perimeter as compared to the circular patch. This patch shape not only reduces the first resonant frequency of the antenna, but also widens its bandwidth towards higher

frequency side due to higher resonant frequencies of distinct segments of the patch boundary. The design methodology of the proposed patch is depicted in Figure 4.1. The flower-shaped radiating patch was designed using four identical petals. Each petal was designed using nine point spline curves and then the resulting structure was rotated by 45^0 to obtain the desired flower-shaped patch shown in Figure 4.1(b) and (c). The proposed radiating patch was excited using 50 Ω CPW and 50 Ω microstrip line (MS) feeds seperately, which are explained in Sections 4.3 and 4.4 of the present chapter respectively.

4.3 CPW-fed Flower-shaped Planar Monopole Antenna (PMA)

4.3.1 *Design of CPW-fed Flower-shaped PMA*

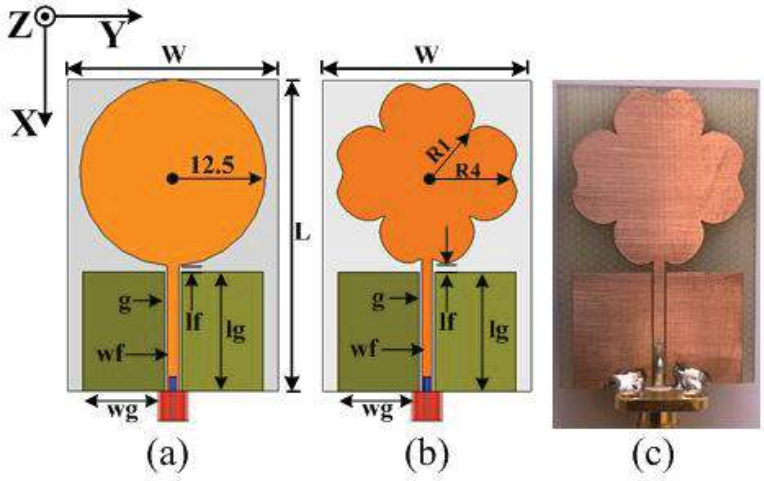

Figure 4.2: Geometries of CPW-fed (a) conventional circular patch antenna, (b) flower-shaped patch antenna; and (c) fabricated antenna.

The geometrical configurations of CPW-fed conventional circular patch and the proposed flower-shaped patch antennas with their shape parameters are shown in Figures 4.2(a) and (b) respectively. The proposed CPW-fed flower-shaped patch antenna was designed using cheap and easily available FR4 substrate having relative dielectric constant 'ε_r' of 4.4 and thickness 'h' of 1.6 mm. The dimensions of the proposed flower-shaped patch antenna along with 50 Ω CPW feed were optimized through simulation using Ansys' HFSS software. The optimized dimensions of the proposed flower-shaped patch antenna and CPW feed are listed in Table 4.1.

Table 4.1: Design parameters of CPW-fed flower-shaped PMA

Parameter	Value (mm)	Parameter	Value (mm)
W	28	R1	8
L	41.8	Rx2	1
wg	11	Ry2	10
lg	16	Rx3	7
wf	1.5	Ry3	10
lf	0.8	R4	8
g	0.3	h	1.6

4.3.2 *Simulation and Measurement of CPW-fed Flower-shaped PMA*

4.3.2.1 Simulation Study

The design and simulation of CPW-fed flower-shaped PMA were carried out using Ansys' HFSS software. The parametric study was conducted to observe the effect of the antenna geometrical parameters on the input VSWR-frequency characteristic bandwidth and determine the optimized VSWR bandwidth of the proposed CPW-fed flower-shaped patch antenna.

The antenna geometrical parameters considered for parametric study are the patch radii 'R1' and 'R4'. Other geometrical parameters of the antenna and the feed are kept constant while considering the effect of specified patch geometrical parameter on the VSWR bandwidth of the proposed antenna. Figure 4.3(a) shows the variation of input VSWR of the antenna with frequency by taking the patch radius 'R1' (corresponding to edge depth) as a parameter. It is seen from Figure 4.3(a) that the upper cutoff frequency of the antenna increases with patch radius 'R1' while little change is observed in the lower cutoff frequency. Further, three VSWR valleys corresponding to antenna resonances each for 'R1' values of 7 and 8 mm are obtained while only two VSWR valleys are observed for 'R1' value of 6 mm. In addition, it is observed that the trend of VSWR variation with frequency is nearly the same for each 'R1' value over the frequency range 2.2−7.5 GHz while this trend changes for higher frequencies (beyond 7.5 GHz) from one 'R1' value to another. It can be inferred from Figure 4.3(a) that larger value of 'R1' reduces the size of distinct boundary segments which results in higher antenna resonant frequencies corresponding to these segments. The optimum value of 'R1' for the

proposed broadband antenna is 8 mm for which VSWR (≤ 2) bandwidth is found to be 4.59:1 (2.2−10.1 GHz).

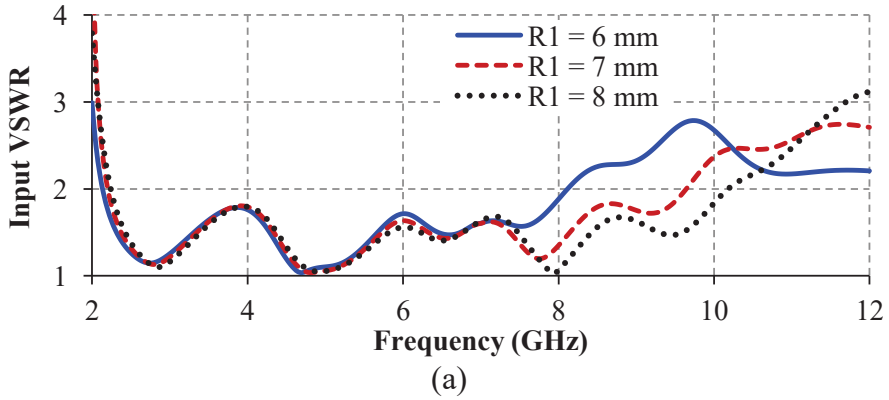

Figure 4.3: The effects of geometrical parameters (a) R1 and (b) R4 on the input VSWR-frequency characteristic of the proposed CPW-fed flower-shaped patch antenna.

Figure 4.3(b) shows the variation of input VSWR of the antenna with frequency by taking the patch radius 'R4' (crresponding to curve depth) as a parameter. It is seen from Figure 4.3(b) that the upper cutoff frequency of the antenna increases with patch radius 'R4'. Further, three VSWR valleys for antenna resonances are obtained within the bandwidth of antenna for each 'R4' value. In addition, it is observed that the resonant frequency corresponding to VSWR valley near 8 GHz increases with 'R4' value. The values of two VSWR peaks near 4 and 7.5 GHz increases with the value of 'R4' while the value of one VSWR peak near 9 GHz decreases with increase in 'R4' value. It can be inferred from Figure 4.3(b) that again larger value of 'R4' reduces the size of boundary segments which results in higher antenna resonant frequencies corresponding to

these segments. The optimum value of 'R4' for the proposed broadband antenna is 8 mm for which VSWR (≤ 2) bandwidth is found to be 4.59:1 (2.2−10.1 GHz).

It is observed from the parametric study that the patch radii 'R1' and 'R4' affect the smaller patch segments. Since the smaller patch segments result in higher resonant frequencies of the antenna, hence by optimizing the patch dimensions 'R1' and 'R4', significant increase in upper cutoff frequency of the antenna (and therefore its operating bandwidth) is obtained.

The optimum dimensions of design parameters of the antenna and 50 Ω CPW feed through simulation are listed in Table 4.1. The antenna with optimum dimensions was then used to obtain its simulated input and far-field characteristics including input VSWR-frequency characteristic, surface current distributions, co- and cross-polar radiation patterns in principal planes, and variations of realized gain and total efficiency versus frequency. Further, time domain analysis of antenna of optimum dimensions was also carried out through simulation using Computer Simulation Technology Microwave Studio (CST MWS) software. For this purpose, a setup was considered in which two identical (proposed) antennas (transmiting and receiving) were placed at a distance of 30 cm (far-field region) in two different orientations, face-to-face and side-by-side. The transmitting antenna was excited with Gaussian pulse and the signal was received at the receiving antenna. Using this setup, the system fidelity factor (SFF) [Quintero *et al.* (2011)] which is a measure of correlation between transmitted and received signals, and group delay-frequency characteristic of the antenna were obtained.

4.3.2.2 Experimental Study

The proposed CPW-fed patch antenna of optimum geometrical dimensions was fabricated the T-Tech make Quick Circuit QC 5000 prototyping machine. The prototype of the fabricated CPW-fed flower-shaped PMA is shown in Figure 4.2(c). The fabricated CPW-fed flower-shaped PMA was tested experimentally over the frequency range 2−12 GHz. The measurement procedures are similar to those for TTLPA (see Sub-section 3.2.3.2). The values of input VSWR over

frequency range of 2−12 GHz were measured using Anritsu make VNA Master Vector Network Analyzer (Model No.: MS2038C). The co- and cross-polar radiation patterns of the proposed CPW-fed flower-shaped PMA in E-plane (xz-plane) and H-plane (yz-plane) were measured in an anechoic chamber at the discrete frequencies of 3, 5, 8 and 10 GHz using experimental setup identical to that given in Sub-section 3.2.3.2. The experimental gain values of the antenna were also obtained at different frequencies over the operating frequency band using comparison method described in Sub-section 3.2.3.2. In addition, group delay-frequency characteristic of the antenna was measured over the operating frequency band using the aforementioned VNA and two identical CPW-fed flower-shaped PMAs. One antenna was used as transmitting antenna and the other antenna acted as receiving antenna in face-to-face and side-by-side configurations at a distance of 30 cm in the far-field region.

The simulated and corresponding measured results for input VSWR-frequency characteristics, radiation patterns, variations of gain in broadside direction and group delay of the antenna versus frequency are compared and discussed in different Sub-sections of Results and Discussion Section 4.3.3.

4.3.3 *Results and Discussion*

4.3.3.1 Input VSWR-Frequency Characteristics

The variations of simulated and measured input VSWR of the proposed antenna with frequency are shown in Figure 4.4. It can be seen from Figure 4.4 that simulated variations of input VSWR of the antenna with frequency determined using Ansys' HFSS and CST MWS softwares are nearly in agreement with each other as well as with the measured characteristic. Further, it is observed from Figure 4.4 that lower cutoff frequencies of the antenna obtained through simulation and measurement are identical while the upper cutoff frequencies differ slightly from one another due to fabrication error. The simulated VSWR bandwidths of the antenna using Ansys' HFSS and CST MWS softwares are found to be 4.59:1 (2.2−10.1 GHz) and 4.75:1 (2.16−10.27 GHz) respectively

whereas measured VSWR bandwidth of the antenna is found to be 4.81:1 (2.2−10.6 GHz).

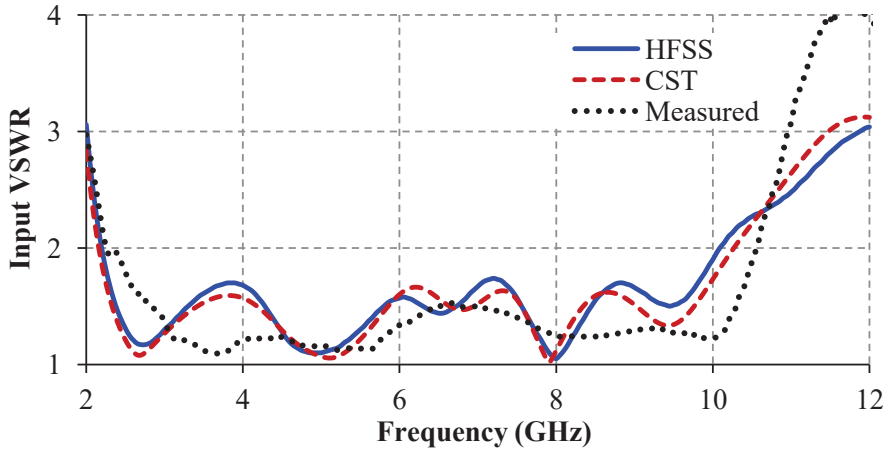

Figure 4.4: Simulated and measured input VSWR-frequency characteristics of proposed CPW-fed flower-shaped antenna.

4.3.3.2 Comparison of Simulated Input VSWR-Frequency Characteristics of Circular Patch and the proposed Flower-shaped Patch Antennas

Figure 4.5 shows the variations of simulated input VSWR of conventional circular patch and the proposed flower-shaped patch antennas with frequency.

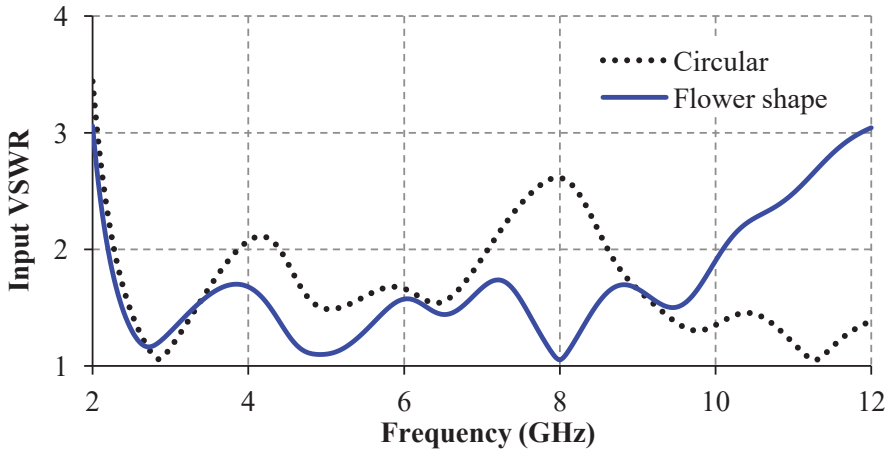

Figure 4.5: Simulated input VSWR-frequency characteristics of the CPW-fed circular patch and the proposed flower-shaped patch antennas.

It is seen from Figure 4.5 that the lower cutoff frequency of flower-shaped antenna is slightly less than the corresponding frequency of circular patch antenna

due to the larger perimeter of flower-shaped patch. In addition, it is observed that the first resonant frequency (= 2.7 GHz) of flower-shaped patch antenna is slightly less as compared with the first resonant frequency (= 2.85 GHz) of circular patch antenna with circular patch radius equal to largest radius of flower-shaped patch. It is noticed that, the circular patch antenna exhibits poor impedance matching (VSWR > 2) in the frequency range 7−8.5 GHz with maximum VSWR at 8 GHz whereas the flower-shaped patch antenna shows good impedance matching (VSWR < 2) in the frequency range 7−8.5 GHz with minimum VSWR at 8 GHz. The impedance mismatch is mitigated by smaller segments of flower-shaped patch antenna. Further, it can noted that the flower-shaped patch itself is capable of providing good impedance match (VSWR ≤ 2) with the 50 Ω CPW feed without any modification of feed line and ground plane over the frequency range 2.2−10.1 GHz (bandwidth = 7.9 GHz).

4.3.3.3 Simulated Surface Current Distributions

Figure 4.6 shows the simulated surface current distributions on the proposed CPW-fed flower-shaped patch antenna at discrete frequencies of 3, 5, 8 and 10 GHz.

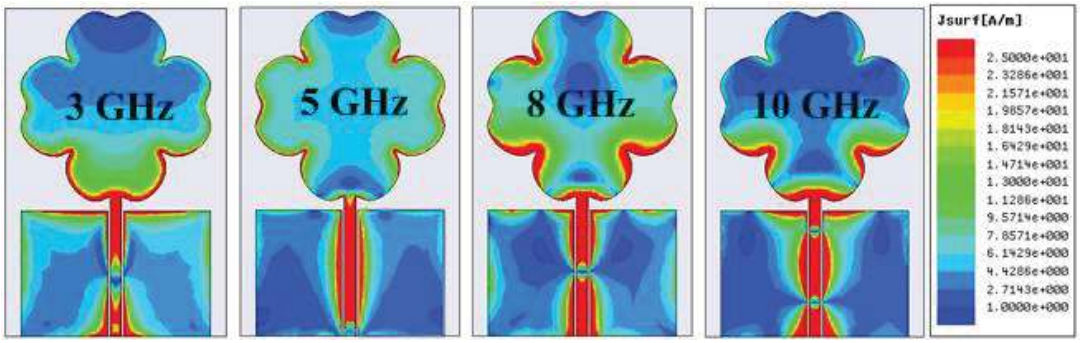

Figure 4.6: Simulated surface current distributions on the proposed CPW-fed flower-shaped patch at 3, 5, 8, and 10 GHz.

It is clear from Figure 4.6 that surface current is concentrated in the outer region of the patch compared to its central region at the frequencies chosen for investigation. It indicates that the antenna radiates from the edges of the patch. At 3 GHz the surface current is distributed around the perimeter of the patch with only one current density minimum occurring in the boundary region at the top of

the patch. As frequency increases, the single current density minimum breaks into a number of current density minima with this number increasing with operating frequency. Further, it is observed that the feed-line has two minima for surface current density at 10 GHz, whereas only single minimum level of surface current density can be seen for lower frequencies of 3, 5, and 8 GHz. This indicates that the path length traveled by current depends on the number of half-wavelengths accommodated in the total length of patch perimeter. As frequency increases, number of half-wavelengths accommodated within the patch perimeter also increases resulting in greater number of maxima and minima of surface current density occurring around the patch perimeter.

4.3.3.4 Radiation Patterns

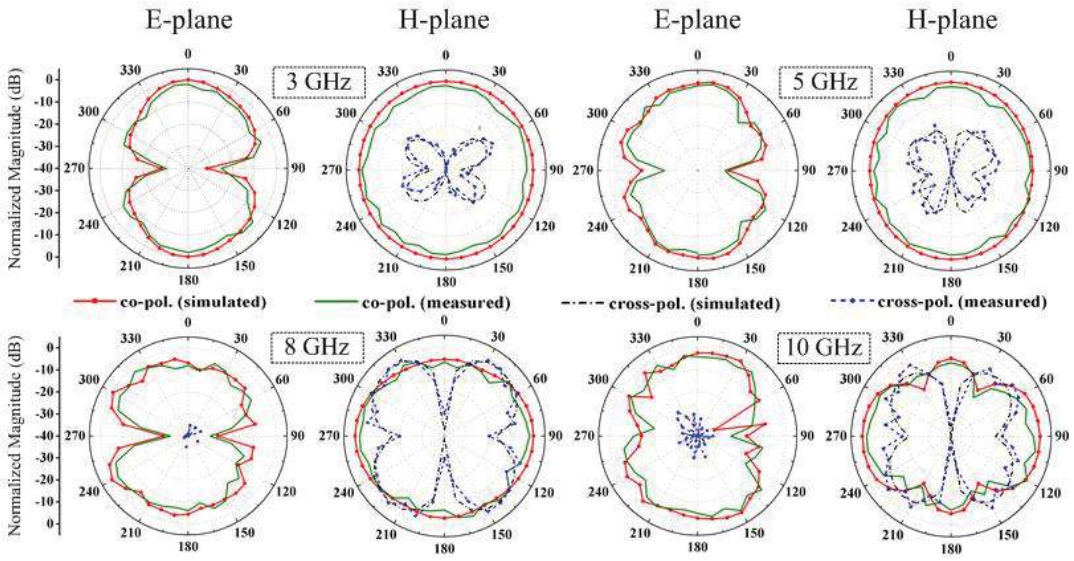

Figure 4.7: Simulated and measured radiation patterns of CPW-fed flower-shaped patch antenna at 3, 5, 8, and 10 GHz.

The simulated and measured radiation patterns (in the form of normalized power versus angle) of the proposed antenna in E-plane (xz-plane) and H-plane (yz-plane) at the discrete frequencies of 3, 5, 8, and 10 GHz are shown in Figure 4.7. It can be seen from Figure 4.7 that simulated radiation patterns are nearly in agreement with the corresponding measured radiation patterns. Further, it can be observed from Figure 4.8 that the antenna shows nearly bidirectional and almost omni-directional co-polar radiation patterns in E- and H-planes respectively. In

addition, it is observed that the radiation patterns are smooth for lower frequencies while the patterns get distorted with increase in operating frequency. It may due to the presence of increasing number of surface current density maxima and minima around the perimeter of patch for higher frequencies. Both simulated and measured E-plane cross-polarization levels lie in the range -35 to -85 dB and -26 to -70 dB respectively for all the frequencies (not visible clearly in the graphs due to the 0 to -40 dB amplitude scale accommodated within limited graph size) whereas the simulated and measured H-plane cross-polarization level lie in the range -1 to -67 dB and -1 to -53 dB respectively and increases with frequency starting from -30 dB at 3 GHz. The maximum measured/simulated cross-polarization level in H-plane reaches 0 dB (for some directions) at 8 and 10 GHz.

4.3.3.5 Realized Gain- and Total Efficiency-Frequency Characteristics

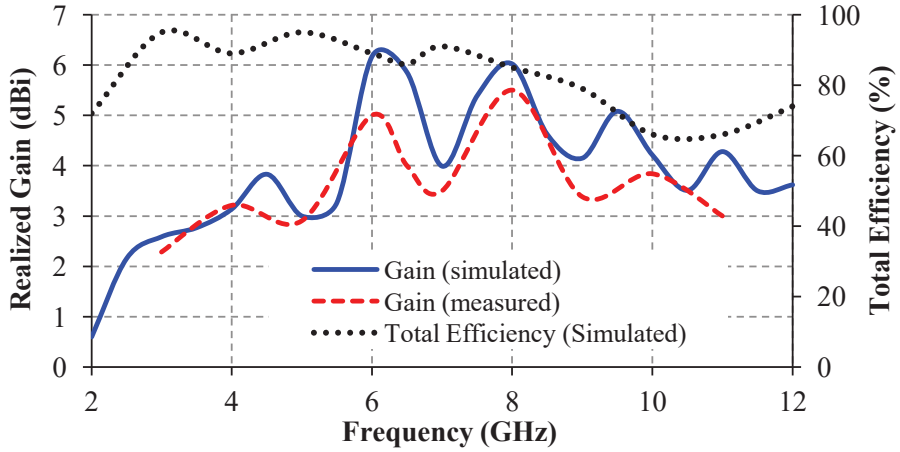

Figure 4.8: Simulated and/or measured realized gain- and total efficiency-frequency characteristics of proposed CPW-fed flower-shaped patch antenna.

The variations of simulated and/or measured maximum realized gain in broadside direction and total efficiency of the antenna with frequency are shown in Figure 4.8. It can be seen from Figure 4.8 that the simulated gain-frequency characteristic is nearly in agreement with the experimental characteristic. In addition, it is observed that the simulated gain values lie in the range 0.6 dBi (at 2 GHz) − 6.2 dBi (at 6.1 GHz) whereas the experimental values of gain vary in the range 2.3 dBi (at 3 GHz) − 5.0 dBi (at 10 GHz) over the operating frequency band of the antenna. The simulated values of total efficiency lie in the range 95 % (at 3

GHz) − 66 % (at 10 GHz) over the operating frequency range. The total efficiency decreases with increase in frequency due to losses related to substrate/connectors.

Fig. 4.8 shows the variation of maximum realized gain in broadside direction with frequency. The realized gain is defined as power gain of the antenna (which is directly proportional to square of the frequency and effective area of the antenna) times the mismatch efficiency of the antenna. Fig. 4.7 shows the radiation patterns normalized to the corresponding maximum gain (power) level (referred to co-polar patterns) at certain angles for different frequencies. Therefore, the realized gain of the antenna of given physical size is dependent on operating frequency, radiation pattern given in Fig. 4.7 and VSWR-frequency characteristic given in Fig. 4.4. The VSWR-frequency characteristic provides the mismatch efficiency of the antenna. Therefore, realized gain given in Fig. 4.8 is linked to radiation pattern in Fig. 4.7 as well as to frequency and VSWR-frequency characteristic given in Fig. 4.4.

More specifically, co-polar radiation pattern is smooth and power level of the pattern at 0^o is maximum (i.e., directive) at lower frequency of 3 GHz and the pattern distorts gradually at higher frequencies. So, the power level of co-polar patterns at 0^o angle varies with frequency. The same can be observed from Fig. 4.7.

The realized gain of the antenna which is a function of frequency, radiation pattern as well as mismatch efficiency. It can be observed from Fig. 4.4 (simulated VSWR-frequency characteristic) that matching is best at 8 GHz, while it degrades gradually while going to frequencies of 5, 3 and 10 GHz in that order. The realized gain shown in Fig. 4.8 is also maximum (6 dBi) at 8 GHz and it degrades to 3 dBi and 2.6 dBi for frequencies of 5 and 3 GHz respectively. Mismatch efficiency is the worst at 10 GHz out of the frequencies considered for study of radiation patterns which will provide reduction in realized gain. But 10 GHz is the highest frequency out of the lot. Considering the foregoing statements and realizing the fact that frequency is dominant factor in affecting the gain of the antenna in general, it can be said that the antenna would provide moderate

realized gain at 10 GHz. Therefore, moderate realized gain of 4.2 dBi for the antenna is observed at 10 GHz.

At lower frequency (3 GHz) where pattern is smooth and impedance matching is good, maximum power level is obtained at 0^o angle which corresponds to the realized gain of 2.6 dBi. At slightly higher frequency (5 GHz), co-polar pattern distorts slightly and maximum power level deviates slightly from 0^o angle which corresponds to realized gain of 3 dBi since matching is better as compared with 3 GHz. At 8 GHz, co-polar pattern distortion is higher and maximum co-polar power level deviated to a large extent from 0^o but the realized gain (= 6 dBi) is highest since the impedance matching is best and operating frequency is higher as compared with 3 and 5 GHz. At 10 GHz (the highest frequency considered for radiation pattern studies) the pattern is highly distorted and greater deviation in maximum co-polar power level from 0^o angle is observed as compared with that at 8 GHz. Though the pattern is greatly distorted and impedance matching is poor, the realized gain (= 4.2 dBi) is moderate since the operating frequency (= 10 GHz) is the highest as compared with the frequencies of 3, 5 and 8 GHz.

4.3.3.6 Effect of Changes in Substrate Parameters with Frequency on Antenna Performance

The dielectric constant of FR-4 substrate material slowly reduces whereas its conductivity increases linearly with increase in frequency over the operating frequency range of the antenna. As substrate dielectric constant reduces by about 0.2 over the operating frequency band of the antenna, the -10 dB reflection coefficient bandwidth would increase slightly [Holzman (2006)]. The slow reduction in dielectric constant of the substrate with increase in frequency would show slight increasing trend in the gain of the antenna with frequency. Further, as thickness of FR-4 substrate material increases, the -10 dB reflection coefficient bandwidth of the antenna would increase due to reduction in its Q-factor. The gain of the antenna would increase with substrate thickness due to generation of more fringing fields from thicker substrate.

With increase in substrate conductivity as frequency increases, the reflection coefficient and gain performance of the antenna with frequency would degrade due to increase in losses. The total efficiency of the antenna would also reduce with frequency due to more losses at higher frequencies whereas insignificant change would be observed in total efficiency due to change in substrate dielectric constant by about 0.2 within the operating frequency range of the antenna.

4.3.3.7 Time Domain Analysis

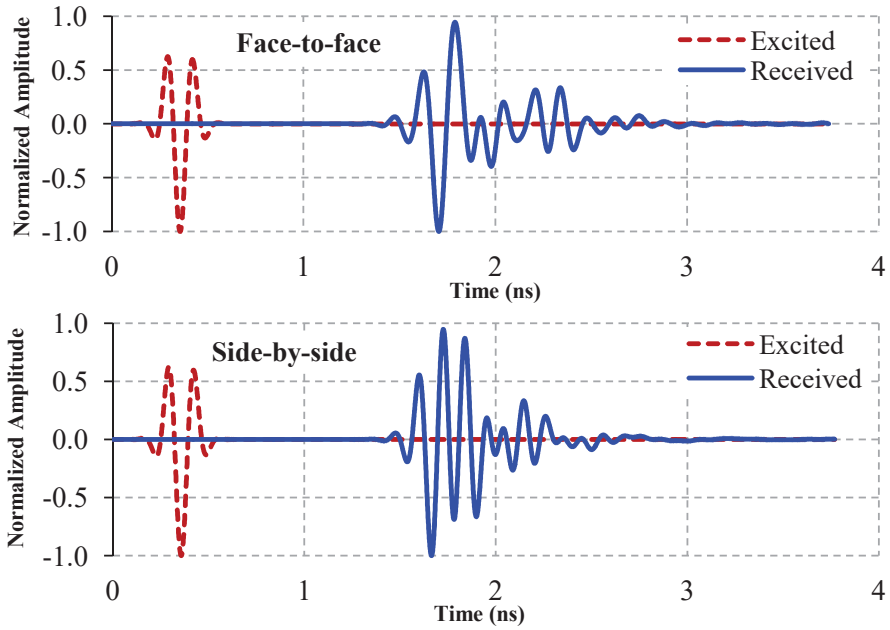

Figure 4.9: Excited and received pulses for face-to-face and side-by-side orientations of proposed CPW-fed flower-shaped patch antennas at a distance of 30 cm.

One of the important performance indicators of broadband antennas is their pulse handling capability. It can be studied through time domain analysis and fidelity factor calculation in the far-field region in face-to-face and side-by-side orientation with respect to transmitting antenna using CST MWS software. The transmitting antenna was excited with Gaussian pulse and the signal was received at the receiving antenna kept at a distance of 30 cm in the far-field region. The normalized amplitudes of excited and received signals are shown in Figure 4.9. This figure depicts that the received pulse is similar to that transmitted, which

indicates that distortion in received signal is insignificant. The correlation between excited and received signals is calculated using system fidelity factor (SFF) [Quintero *et al.* (2011)]. The system fidelity factors (SFFs) in the case of face-to-face and side-by-side orientations are found to be 0.75 and 0.72 respectively. The calculated SFF values are close to unity showing that the antenna has good pulse handling characteristics.

Another important parameter of broadband antennas is their almost constant group delay over the whole operating frequency band. The group delay is used to represent the degree of pulse signal distortion. The simulated values of far-field group delay was obtained using arrangements of transmitting and receiving antennas identical to those employed for time domain analysis explained earlier. The variations of far-field group delay of the proposed antenna for face-to-face and side-by-side configurations with frequency were determined through simulation using CST MWS software and the results are provided in Figure 4.10. It can be seen from Figure 4.10 that the simulated values of far-field group delay of the proposed antenna vary in the range 0.5−2 ns for face-to-face and side-by-side configurations over the whole operating frequency band.

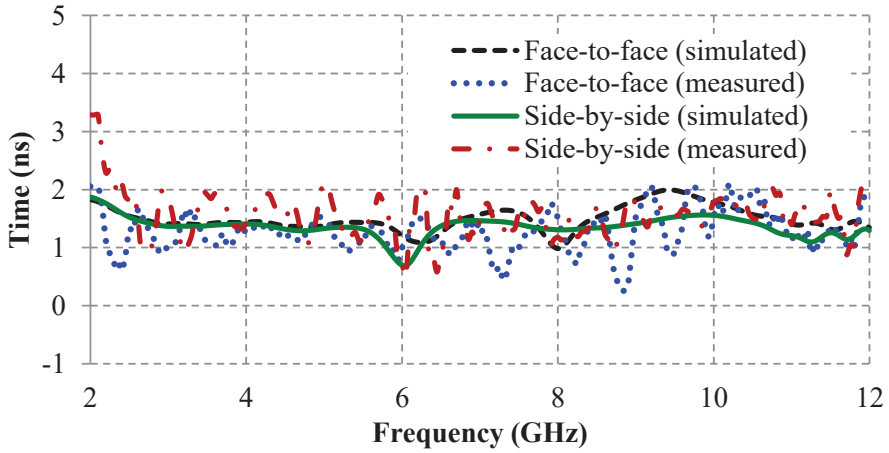

Figure 4.10: Far-field group delays of CPW-fed flower-shaped patch antenna for different orientations at a distance of 30 cm.

The values of far-field group delay of the proposed antenna at discrete frequencies for face-to-face and side-by-side configurations were mesured and the experimental results are shown in Figure 4.10. It can be seen from Figure 4.10

that values of measured group delay of the proposed antenna vary in the range 0.5−2 ns for face-to-face and side-by-side configurations over major portion of the operating frequency band. The deviation in the measured and simulated values of group delay may be due to the fabrication and manual measurement errors.

4.4 Microstrip Line-fed Flower-shaped Planar Monopole Antenna (PMA)

4.4.1 *Design of Microstrip Line (MS)-fed Flower-shaped PMA*

The geometrical configuration of the microstrip line-fed proposed flower-shaped patch antenna (MS-fed antenna) along with its shape parameters is shown in Figure 4.12(a). Initially, the 50 Ω straight microstrip line and rectangular partial ground were considered. Subsequently, the straight microstrip line was tapered to increase the line impedance so that antenna input impedance can be properly matched to tapered microstrip line and hence to the 50 Ω coaxial cable feed. The rectangular partial ground plane was changed to semi-circular shape and then to semi-elliptical shape to improve impedance matching between the antenna and the 50 Ω feed. The aforesaid statements are arranged in steps called antenna design steps depicted in Figure 4.11. The antenna and the feed were designed on 1.6 mm thick FR4 substrate having dielectric constant of 4.4.

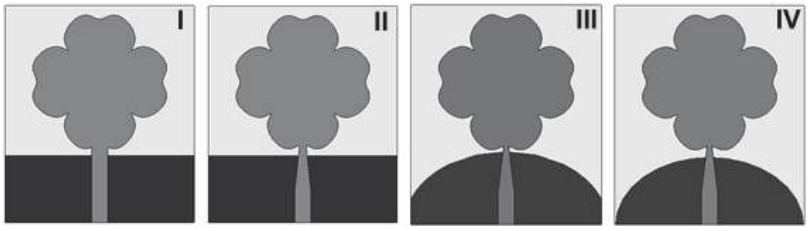

Figure 4.11: Design steps concerning MS-fed flower-shaped patch antenna.

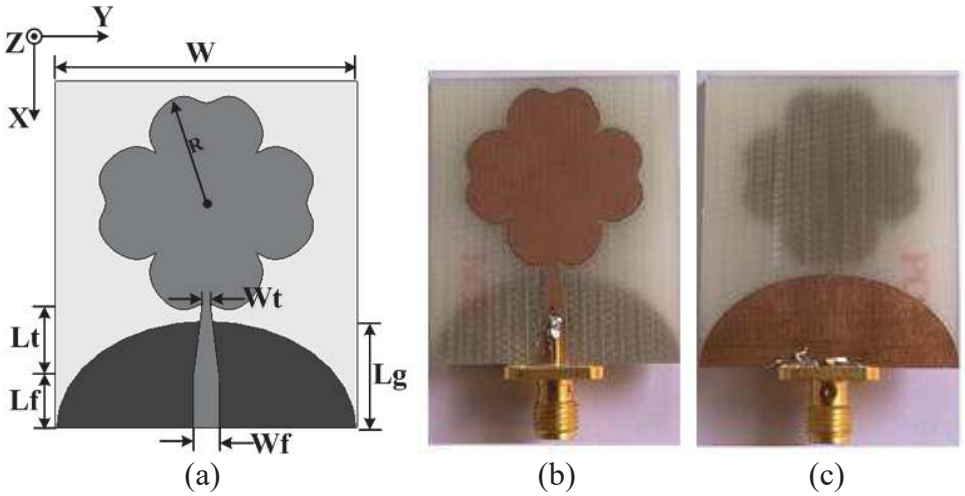

Figure 4.12: MS-fed flower-shaped patch antenna (a) geometry, (b) front view of prototype, and (c) back view of prototype.

The optimum dimensions of antenna and 50 Ω microstrip line feed obtained through simulation using Ansys' HFSS software are listed in Table 4.2.

Table 4.2: Design parameters of MS-fed flower-shaped PMA

Parameter	Value (mm)	Parameter	Value (mm)
W	34	R1	8
Wt	1.4	Rx2	1
Wf	3	Ry2	10
L	39.1	Rx3	7
Lt	8.56	Ry3	10
Lf	5.4	R4	8
Lg	12	R	12.5

4.4.2 *Simulation and Measurement of MS-fed Flower-shaped PMA*

4.4.2.1 Simulation Study

The simulation study of MS-fed flower-shaped PMA was carried out using Ansys' HFSS software and the optimum dimensions of the antenna and 50 Ω feed are listed in Table 4.2. The MS line-fed antenna of optimum dimensions was then used to obtain its simulated input and radiation characteristics, which include input VSWR-frequency characteristic, surface-current distributions, co- and cross-polar radiation patterns in principal planes and variations of realized gain in broadside direction and total efficiency of the MS-fed antenna with frequency. In addition, time domain analysis of the antenna having optimum dimensions was performed using CST MWS software as provided in Sub-section 4.3.2.1 and in reference [Quintero *et al.* (2011)]. The simulated system fidelity factors (SFFs) for face-to-face and side-by-side configurations of the proposed antennas were calculated and simulated variation of group delay of the proposed antenna versus frequency was obtained as described in Sub-section 4.3.2.1 and in reference [Quintero *et al.* (2011)].

4.4.2.2 Experimental Study

The proposed antenna was fabricated using T-Tech make Quick Circuit QC 5000 prototyping machine as per design specifications. The front and back views of the fabricated antenna along with the tapered microstrip line feed and partial

ground plane are shown in Figure 4.12(b) and (c) respectively. The fabricated MS-fed flower-shaped PMA was tested experimentally over the frequency range 2−14 GHz. The input VSWR-frequency characteristic, radiation patterns and realized gain-frequency characteristic of the antenna were determined experimentally adopting procedures identical to those discussed earlier in Section 4.3 for CPW-fed antenna.

The simulated and corresponding experimental results for input VSWR-frequency characteristic, radiation patterns in H- and E-planes and gain-frequency characteristics of the antenna were compared and discussed in different Sub-sections of Results and Discussion Section 4.4.3. In addition, the performance of flower-shaped PMAs excited using both CPW and microstrip line feeds are also compared.

4.4.3 *Results and Discussion*

4.4.3.1 Effects of Shape of Feed Line and Ground Plane on Input VSWR-Frequency Characterstics of the MS-fed Flower-shaped Patch Antenna

The effects of various configurations of microstrip line feed and ground plane on input VSWR-frequency characteristic of the MS-fed antenna were studied through simulation using Ansys' HFSS software. Figure 4.13 shows the simulated variations of input VSWR of the antenna versus frequency for various configurations of microstrip line feed and ground plane. First configuration pertains to the flower-shaped patch with 50 Ω microstrip line feed of width = 3 mm, and rectangular ground plane of size 34 × 12.1 mm^2. It is observed from Figure 4.14 that first antenna configuration operates in two split frequency bands for input VSWR ≤ 2 over the frequency range 2−14 GHz. This might have occurred due to poor impedance matching between the feed line and the patch antenna in certain frequency bands as well as to the presence of rectangular ground plane.

In the second configuration, tapered microstrip line is used with wf = 3 mm and wt = 1.4 mm while the ground plane remains rectangular in shape. It is

observed that for second antenna configuration, input VSWR is less than or equal to 2 over wider range of frequencies except for frequencies near 6.2 and 13.5 GHz, where its value is slightly greater than 2. It may be due to the use of tapered section of microstrip line feed, which makes the line impedance approximately equal to input impedance at the edge of the patch and hence providing improved impedance matching over wider frequency range.

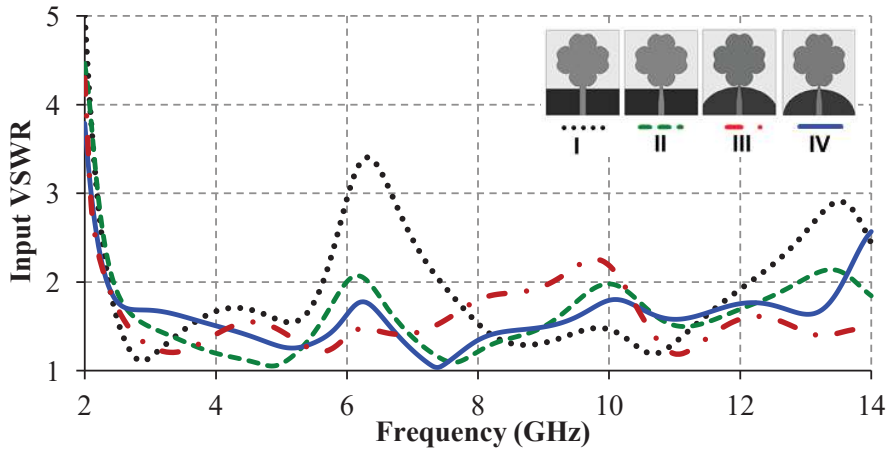

Figure 4.13: Simulated input VSWR-frequency characteristics of the proposed MS-fed flower-shaped patch antenna for different configurations of feed line and ground plane.

In third configuration, the tapered microstrip line is identical to that used in the second configuration while the ground plane is curved making it semicircular, which further improves the impedance matching. It is observed from Figure 4.13 that third antenna configuration operates over wider frequency range as compared with second configuration but the antenna impedance is slightly mismatched to the input line at frequencies near 10 GHz for which input VSWR is slightly greater than 2. It is to be noted that values of input VSWR of the third antenna configuration are less than 2 for frequencies near 6.2 and 13.5 GHz, where the values are slightly greater than 2 for the second configuration.

In the fourth and final configuration, identical tapered microstrip line as used in second and third configurations was employed and the ground plane was further curved, which results in semi-elliptical ground plane. It is observed from Figure 4.13 that fourth antenna configuration is matched to the input line (input

VSWR ≤ 2) over broadest frequency range 2.3−13.6 GHz. Broadband matching for fourth antenna configuration is made possible due to the desirable characteristics of tapered microstrip line and semi-elliptical ground plane. It is also observed that lower cutoff frequency is approximately the same in all antenna configurations, because it depends on the size of perimeter of the flower-shaped patch. It may be noted here that higher resonant frequencies are achieved due to distinct smaller boundary segments.

4.4.3.2 Input VSWR-Frequency Characteristics

The variations of simulated input VSWR of the proposed optimized MS-fed antenna (fourth configuration) and the CPW-fed antenna with frequency are shown in Figure 4.14.

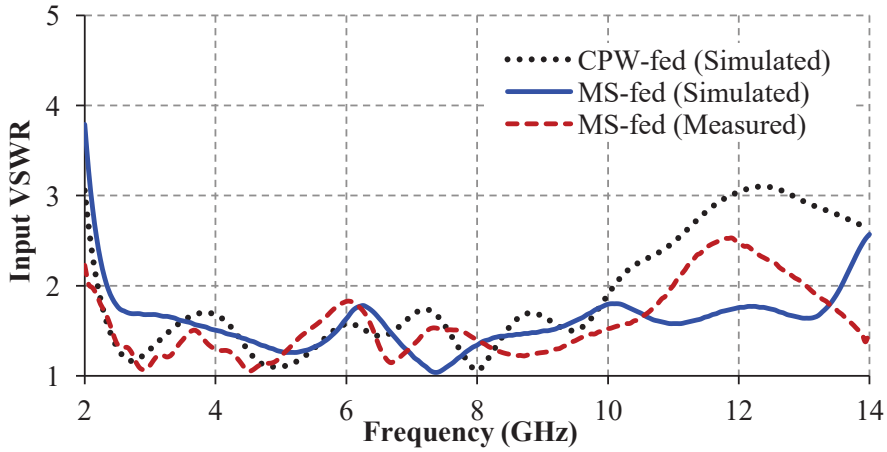

Figure 4.14: Simulated and measured input VSWR-frequency characteristics of the proposed MS-fed and CPW-fed flower-shaped patch antennas.

It is observed that the proposed MS-fed antenna is capable of providing wider bandwidth with slightly increased lower cutoff frequency as compared to CPW-fed antenna. Further, the variation of input VSWR of fabricated (proposed) antenna with frequency was determined experimentally and the measured results are compared with corresponding simulation results (Figure 4.14). It is seen from Figure 4.14 that measured input VSWR-frequency characteristic of the antenna is slightly shifted towards lower frequency side as compared with corresponding simulated characteristic. The measured lower cutoff frequency is found to be 2.1

GHz while the simulated lower cutoff frequency is 2.3 GHz. The simulated and measured upper cutoff frequencies of the antenna are respectively equal to 13.6 and 11.1 GHz. The deviation in simulated and measured upper cutoff frequencies of the antenna might have occurred due to error in fabrication of the small and sharp junctions of tapered line and flower-shaped patch because smaller and sharp edges of the antenna resonate at higher frequencies**.**

4.4.3.3 Simulated Current Distributions

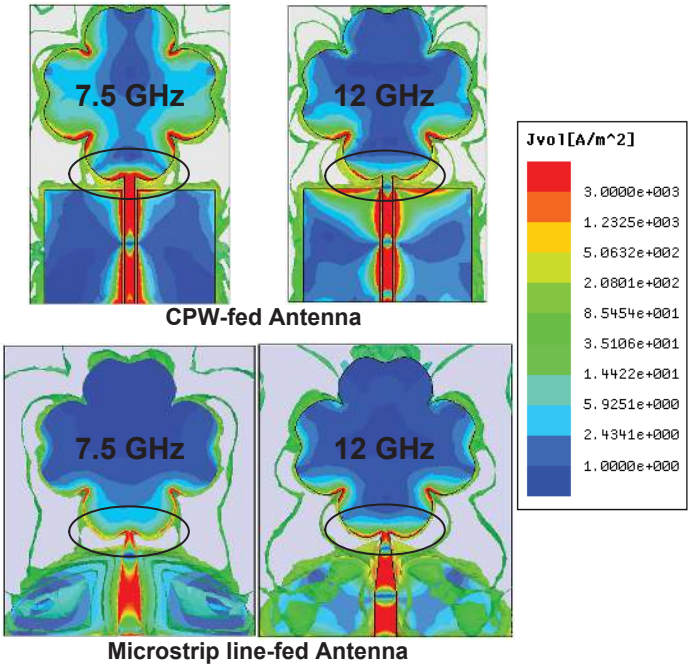

Figure 4.15: Simulated surface and volume current distributions on the proposed MS-fed and CPW-fed flower-shaped patch antennas.

The simulated current distributions on the surfaces of the proposed MS-fed and CPW-fed antennas are shown in Figure 4.15. It is clear from Figure 4.15 that the proposed MS-fed antenna, which has tapered feed line and semi-elliptical ground plane provides wider bandwidth as compared with CPW-fed antenna. The enhanced bandwidth characteristics of the proposed MS-fed antenna can be understood with the help of leaky-wave concept wherein interaction between the patch and feed line as well as ground plane occurs through leaky-wave. The leaky-wave can be depicted in terms of leakage current [Nguyen *et al.* (2012)], which is unwanted current flowing from patch to ground plane through the

substrate. This current can be investigated using volume current distributions on the antenna substrate. Surface and volume current distributions on both antennas at 7.5 GHz (where input VSWR is minimum for the proposed MS-fed antenna) and 12 GHz (where input VSWR is maximum for the CPW-fed antenna) are shown in Figure 4.15. It is observed from Figure 4.15 that for a given antenna, leakage current increases with increase in frequency. Further, it can be investigated that the leakage current is reduced in the feed region (area encircled by ellipse in Figure 4.15) of proposed MS-fed antenna as compared to CPW-fed antenna. So, enhanced bandwidth (towards higher frequency side) obtained for proposed MS-fed antenna may be due to the reduced leakage current in it.

4.4.3.4 Radiation Patterns

The co-polar and cross-polar radiation patterns of the proposed MS-fed antenna in E-plane (xz-plane) and H-plane (yz-plane) with power (at any angle) normalized with respect to maximum power were determined through simulation and experimentally at 3, 6, 9 and 12 GHz and the results are shown in Figure 4.16.

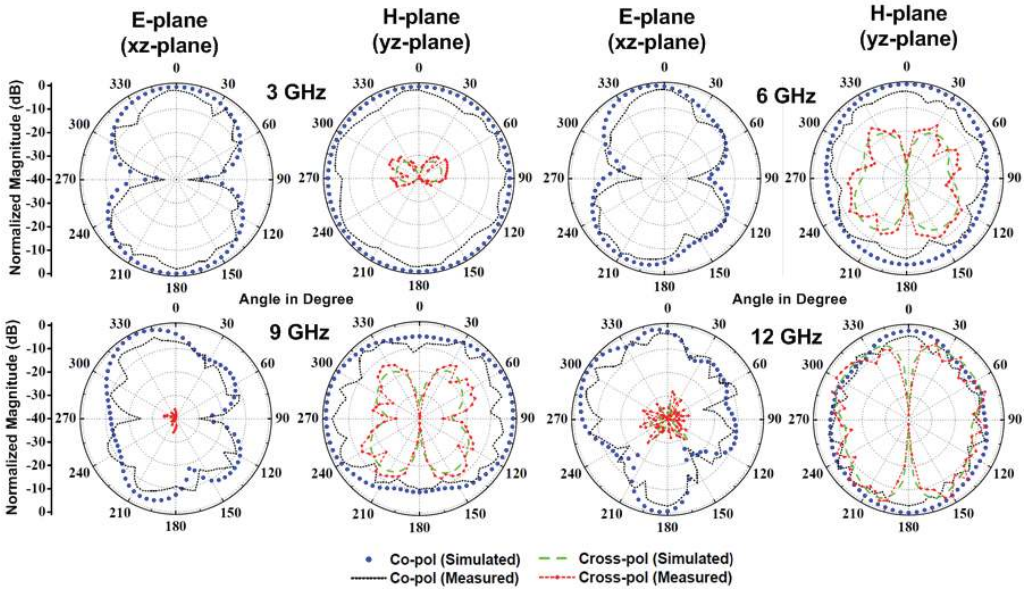

Figure 4.16: Simulated and measured radiation patterns of the proposed MS-fed antenna at 3, 6, 9, and 12 GHz.

It is observed from Figure 4.16 that the simulated radiation patterns of the proposed MS-fed antenna at a given frequency are nearly in agreement with the

respective experimental radiation patterns. Further, the antenna provides nearly bidirectional and almost omni-directional co-polar patterns in E- and H-planes respectively. The radiation patterns of the proposed MS-fed antenna and CPW-fed antenna as shown in Figures 4.16 and 4.7 are similar. The antenna patterns get distorted with increase in frequency due to the generation of higher order modes. The cross-polarized lobe levels of the proposed antenna in both planes increase with frequency. In E-plane, cross-polar levels are insignificant (lying below -40 dB) at 3 and 6 GHz and therefore they are not visible in Figure 4.16. Further, at a given frequency and angle, this level is greater in H-plane than the corresponding level in E-plane.

4.4.3.5 Realized Gain and Total Efficiency-Frequency Characteristics

The variations of realized gain in broadside direction and total efficiency of the proposed MS-fed and CPW-fed antennas versus frequency were studied through simulation using Ansys' HFSS software and values of gain of the antenna at different frequencies within its operating frequency band were measured. The simulation and experimental results for the antenna are presented in Figure 4.17.

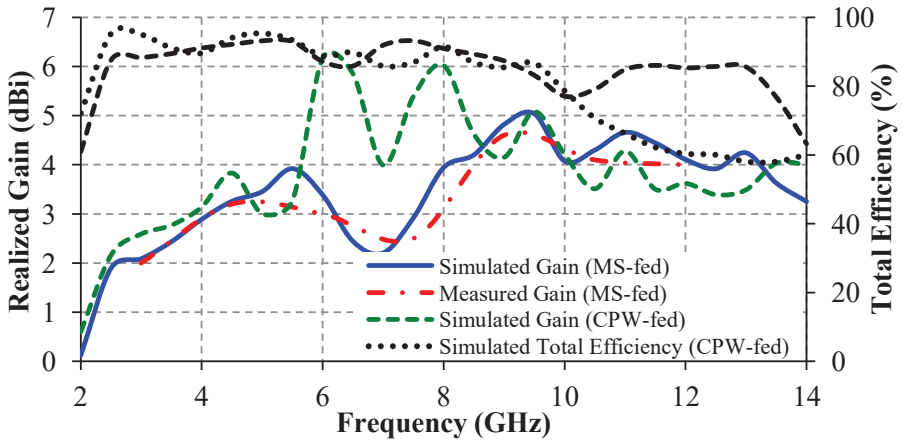

Figure 4.17: Realized gain- and total efficiency-frequency characteristics of the proposed MS-fed and CPW-fed antennas.

It is observed from Figure 4.17 that simulated gain values of the proposed MS-fed antenna are nearly in agreement with the corresponding experimental results over the frequency range used for measurement. Further, it is observed

from Figure 4.17 that the simulated values of realized gain of the proposed MS-fed antenna lie in the range 0.21 dBi (at 2 GHz) − 5.03 dBi (at 9.5 GHz) and simulated values of total efficiency lie in the range 93 % (at 5 GHz) − 63 % (at 14 GHz) over the operating frequency range. It is clear through comparison of variations of gain and total efficiency of both the antennas with frequency that the proposed MS-fed antenna provides variation of gain with frequency equivalent to that of CPW-fed antenna over significant portion of the operating frequency band while its total efficiency values over the operating frequency band are almost equal to or greater than those provided by the CPW-fed antenna. The total efficiency of both antennas decreases with increase in frequency due to increase in substrate losses with frequency. The effect of changes in substrate parameters with frequency on antenna performance would be similar as discussed in earlier sub-section 4.3.3.6.

4.4.3.6 Time Domain Analysis

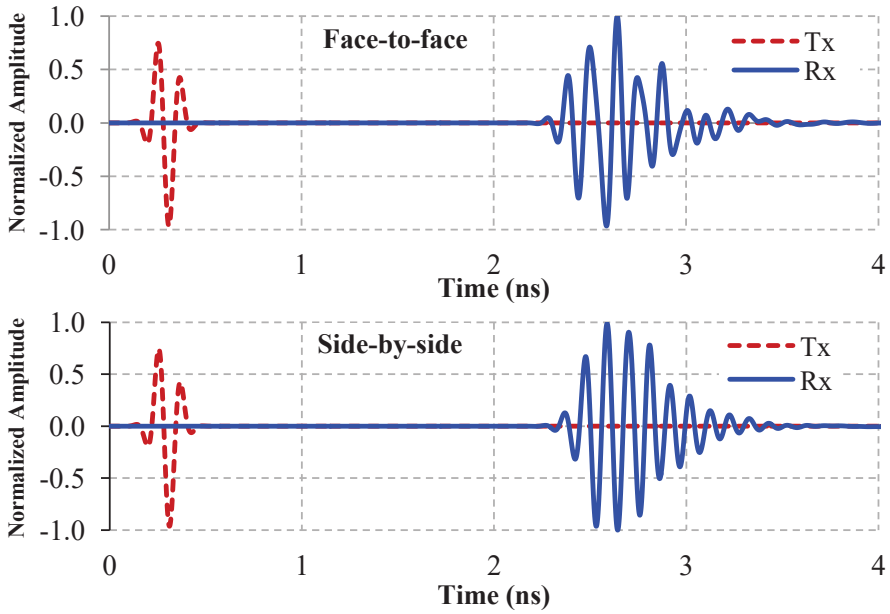

Figure 4.18: Excited and received pulses for face-to-face and side-by-side orientations of MS-fed flower-shaped patch antennas at a distance of 30 cm.

Time domain analysis in face-to-face and side-by-side configurations through simulation using CST MWS software were also done for MS-fed antenna. The normalized signal amplitudes of Gausian pulse transmitted by transmitting antenna and the signal received by the receiving antenna for both

face-to-face and side-by-side configurations are shown in Figure 4.18. It is clear from this figure that the received pulse is quite similar to that transmitted in both configurations. The degree of similarity also known as correlation between excited and received signals is calculated using system fidelity factor [Quintero *et al.* (2011)]. The system fidelity factors in case of face-to-face and side-by-side orientations of MS-fed antennas found to be 0.72 and 0.75 respectively.

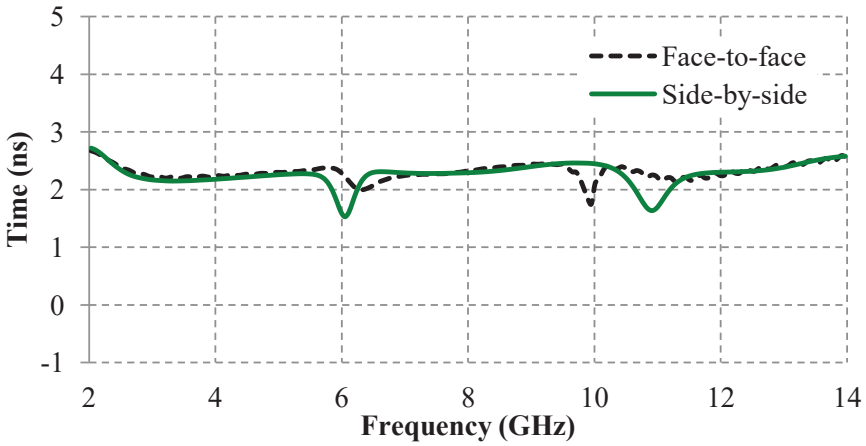

Figure 4.19: Simulated far-field group delays of MS-fed flower-shaped patch antenna for different orientations at a distance of 30 cm.

Figure 4.19 depicts the variations of simulated far-field group delay with frequency of MS-fed antennas in face-to-face and side-by-side configurations with frequency. It is observed from Figure 4.19 that variations of group delay of MS-fed antenna are nearly stable at ~ 2 ns with a variation of 1 ns (from 1.5−2.5 ns) over the whole operating frequency range in both face-to-face and side-by-side configurations. The nearly stable group delay within the operating frequency band shows that the antenna receives wideband Gaussian pulse with very low group delay distortion.

Table 4.3: Comparison of SFF and Group Delay of CPW- and MS-fed flower-shaped PMAs

Parameter	Configuration	CPW-fed Antenna	MS-fed Antenna
SFF	Face-to-Face	0.75	0.72
	Side-by-side	0.72	0.75
Group Delay	Face-to-Face	1.5 ns	1 ns
	Side-by-side	1.5 ns	1 ns

The simulated time domain behavior of both CPW- and MS-fed flower-shaped PMAs are summarized in Table 4.3. It is clear from Table 4.3 that system fidelity factor (SFF) of both CPW- and MS-fed flower-shaped antennas in both face-to-face and side-by-side configurations is more than or equal to 0.72 while the group delay variation with frequency for MS-fed antenna is less as compared to CPW-fed antenna in both face-to-face and side-by-side configurations.

4.5 Summary

In this chapter, flower-shaped planar monopole antenna (PMA) having curved boundary and multiple sub-sections has been investigated using two types of feed line: CPW and microstrip line (MS). In the beginning, input characteristic of the CPW-fed flower-shaped patch antenna has been compared with the characteristic of a CPW-fed circular patch antenna of same outer radius. The proposed CPW-fed flower-shaped patch antenna has been found to have (i) less lower cutoff frequency due to its larger perimeter, and (ii) wider VSWR bandwidth due to its larger perimeter as well as distinct smaller boundary segments of flower-shaped patch, as compared with the circular patch antenna. The arrangement of CPW feed and ground plane has been found to act as an impedance matching circuit for patch antenna.

Further, MS-fed flower-shaped patch antenna with various configurations of the microstrip line feed and ground plane has been discussed. It has been found that the proposed flower-shaped patch antenna along with tapered microstrip line and semi-elliptical partial ground plane provides the broadest bandwidth among all the configurations considered in the study. Subsequently, its performance has been compared with that of CPW-fed flower-shaped antenna. The final MS-fed flower-shaped antenna has been found to have enhanced impedance bandwidth as compared with the CPW-fed flower-shaped antenna due to weaker leakage current. The radiation patterns of both antennas are omni-directional and bidirectional in H- and E-planes respectively. The final MS-fed flower-shaped antenna provides reasonable gain, higher total efficiency, similar SFF and lesser far-field group delay with slightly increased antenna size than the CPW-fed

flower-shaped antenna. Owing to these characteristics, the flower-shaped patch antenna along with tapered microstrip line feed and semi-elliptical partial ground plane providing enhanced bandwidth and total efficiency is superior to CPW-fed flower-shaped antenna and can be a good candidate for systems, which utilize ultrawideband (UWB) frequency spectrum along with Bluetooth frequency band.

After investigating nature inspired flower-shaped planar broadband antenna in the present chapter, the castor leaf-shaped quasi-self-complementary antenna and its use as broadband multiple-input-multiple-output (MIMO) antenna with band-rejection characteristic are taken up for investigation in the next chapter.